

Effect of metal solvent and growth surface on boron doping efficiency and impurity incorporation in HPHT-grown diamond single crystals

Hongbo Li(李鸿波), Wenhao Wang(王文豪), Yadong Li(李亚东), Liangchao Chen(陈良超), Zhuangfei Zhang(张壮飞), Yuewen Zhang(张跃文), Qianqian Wang(王倩倩), Biao Wan(万彪), Chunlei Du(杜春雷), and Chao Fang(房超)

Citation: Chin. Phys. B, 2025, 34 (**11**): 118101. DOI: 10.1088/1674-1056/adfb55
http://cpb.iphy.ac.cn; http://iopscience.iop.org/cpb

What follows is a list of articles you may be interested in

Synthesis of two-dimensional diamond by phase transition from graphene at atmospheric pressure

Songyang Li(李松洋), Zhiguang Zhu(朱志光), Youzhi Zhang(张有志), Chengke Chen(陈成克), and Xiaojun Hu(胡晓君)

Chin. Phys. B, 2025, 34 (**5**): 058101. DOI: 10.1088/1674-1056/adb688

Synthesis and nitrogen content regulation of diamond in a high-pressure hydrogen-rich environment

Guofeng Huang(黄国锋), Liangchao Chen(陈良超), and Chao Fang(房超)

Chin. Phys. B, 2024, 33 (**6**): 068102. DOI: 10.1088/1674-1056/ad2a6d

High performance trench diamond junction barrier Schottky diode with a sidewall-enhanced structure

Ying Zhu(朱盈), Wang Lin(林旺), Dong-Shuai Li(李东帅), Liu-An Li(李柳暗), Xian-Yi Lv(吕宪义), Qi-Liang Wang(王启亮), and Guang-Tian Zou(邹广田)

Chin. Phys. B, 2023, 32 (**8**): 088101. DOI: 10.1088/1674-1056/acc2ae

Two-step high-pressure high-temperature synthesis of nanodiamonds from naphthalene

Tong Liu(刘童), Xi-Gui Yang(杨西贵)†, Zhen Li(李振), Yan-Wei Hu(胡宴伟), Chao-Fan Lv(吕超凡), Wen-Bo Zhao(赵文博), Jin-Hao Zang(臧金浩)‡, and Chong-Xin Shan(单崇新)§

Chin. Phys. B, 2020, 29 (**10**): 108102. DOI: 10.1088/1674-1056/abad1c

Inclusions in large diamond single crystals at different temperatures of synthesis

Fei Han(韩飞), Shang-Sheng Li(李尚升), Xue-Fei Jia(贾雪菲), Wei-Qin Chen(陈玮琴), Tai-Chao Su(宿太超), Mei-Hua Hu(胡美华), Kun-Peng Yu(于昆鹏), Jian-Kang Wang(王健康), Yu-Min Wu(吴玉敏), Hong-An Ma(马红安), Xiao-Peng Jia(贾晓鹏)

Chin. Phys. B, 2019, 28 (**2**): 028103. DOI: 10.1088/1674-1056/28/2/028103

SPECIAL TOPIC — Structures and properties of materials under high pressure

Effect of metal solvent and growth surface on boron doping efficiency and impurity incorporation in HPHT-grown diamond single crystals

Hongbo Li(李鸿波)[1], Wenhao Wang(王文豪)[1], Yadong Li(李亚东)[2], Liangchao Chen(陈良超)[1,†], Zhuangfei Zhang(张壮飞)[1], Yuewen Zhang(张跃文)[1], Qianqian Wang(王倩倩)[1], Biao Wan(万彪)[1], Chunlei Du(杜春雷)[2], and Chao Fang(房超)[1,‡]

[1] *Key Laboratory of Material Physics of Ministry of Education, School of Physics and Laboratory of Zhongyuan Light, Zhengzhou University, Zhengzhou* 450052, *China*

[2] *College of Electronic Information Engineering, Yangtze Normal University, Chongqing* 408100, *China*

(Received 14 May 2025; revised manuscript received 11 August 2025; accepted manuscript online 14 August 2025)

To enhance boron doping efficiency and reduce metal impurities in diamonds, selecting an appropriate metal solvent is essential for producing p-type diamonds using the high-pressure high-temperature (HPHT) method. This paper presents a detailed study of the properties and characteristics of boron-doped diamond (BDD) single crystals grown using FeNi and FeCo solvents through the HPHT method. The results indicate that, with the same TiB_2 addition ratio, BDD crystals grown using FeCo solvent have a higher concentration of uncompensated boron ions, resulting in improved boron doping efficiency. Additionally, by growing BDD in the same synthesis environment (FeCo-3 wt% TiB_2) using (111) and (100) seed crystals as growth surfaces, it was found that the boron content in the crystal grown from the (100) seed crystal was higher than that in the crystal grown from the (111) seed crystal. Additionally, the crystals grown with the FeCo solvent contained fewer metal elements (Fe and Co) compared to those produced with the FeNi solvent (Fe and Ni), which supported the growth of high-quality BDD single crystals. This indicated that the choice of growth planes significantly influences the incorporation of boron in diamonds. Our findings hold significant research value for the development of high-quality p-type diamond semiconductors using the HPHT method.

Keywords: boron doping, diamond single crystal, high-pressure high-temperature (HPHT), metal solvent

PACS: 81.05.ug, 74.62.Dh, 61.72.S–, 67.80.dj

DOI: 10.1088/1674-1056/adfb55 **CSTR:** 32038.14.CPB.adfb55

1. Introduction

Diamond is a highly functional material known for its remarkable properties, including exceptional hardness,[1] superior thermal conductivity,[2] a wide bandgap,[3] and high carrier mobility.[4] It also has excellent electrical insulation properties,[5] optical transmittance,[6] and chemical stability.[7] These characteristics contribute to diamond's reputation in the semiconductor[4] industry, where it is valued for its ability to perform effectively under extreme conditions. Specifically, diamond is used in the manufacture of high-power electronic devices[8] and high-temperature electronics,[9] where it maintains stable performance even at elevated temperatures.

Introducing a specific concentration of boron impurities into diamond can impart p-type semiconductor properties.[10] This modification plays a crucial role in enhancing the application of diamonds in electronic components. However, despite its potential, large-scale production and application of boron-doped diamond (BDD) face several challenges and limitations.[11] The crystal defects introduced during boron doping can result in high bulk resistivity, low carrier concentration, and reduced mobility.[12] Currently, chemical vapor deposition (CVD) and high-pressure high-temperature (HPHT) methods are primarily used to produce BDD.[13] Recent research on p-type semiconductor diamonds, both domestically and internationally, has focused mainly on the production of boron-doped films.[14] These p-type diamond films are synthesized using CVD, with boron serving as an additive,[15] and they have been successfully applied in various applications. Microwave plasma chemical vapor deposition (MPCVD) technology has emerged as a leading method for preparing single-crystal diamonds. Its advantages include minimal pollution from microwave energy and the use of pure gas raw materials, making it one of the most promising techniques for producing large, high-quality single-crystal diamonds.[16,17] Despite its advantages, the application of MPCVD for single-crystal diamond production is limited by its low growth rate (approximately 10 μm/h)[18] and high defect density (ranging from 10^3 to 10^7 cm^{-2}).[19,20] These factors significantly hinder its widespread use in various applications. Relative to the CVD method, the HPHT technique of-

†Corresponding author. E-mail: chenlc@zzu.edu.cn

‡Corresponding author. E-mail: fangchao1989@zzu.edu.cn

© 2025 Chinese Physical Society and IOP Publishing Ltd. All rights, including for text and data mining, AI training, and similar technologies, are reserved.

fers a faster growth rate and lower costs for producing single-crystal diamonds, enabling mass industrial production. Additionally, one of its key advantages is the relatively low defect density of diamonds synthesized using HPHT (ranging from 10^3 to 105 cm^{-2}), which theoretically allows for the production of defect-free single-crystal diamonds.[21] Currently, the primary challenges in the HPHT synthesis of BDD are achieving a uniform distribution of boron within the crystal[22] and managing the effects of metal impurities. Synthesizing high-quality single-crystal BDD using the HPHT method for functional applications has become a critical scientific challenge that researchers, both domestically and internationally, are eager to address.

BDD can be synthesized using two HPHT systems, one using metal-containing solvents and another using metal-free solvents. In metal-free solvent systems, graphite-boron composite (GBC) or boron carbide (B_4C) can be employed as precursors for synthesis, but this method requires higher pressure and temperature conditions (usually $P > 8$ GPa, $T >$ 2000 °C),[23–25] and the products are usually small-sized diamonds or polycrystalline diamonds. In contrast, the use of transition metal solvents such as iron (Fe), nickel (Ni), manganese (Mn), and cobalt (Co) can significantly reduce the synthesis conditions ($P = 5$–6 GPa, $T = 1200$–1400 °C).[26] It has been shown that these transition metals have a specific chemical affinity with boron, and this interaction can directly affect the doping efficiency of boron in diamond lattices under HPHT conditions.[27,28] To prepare large BDD single crystals, FeNi and FeCo alloy solvents are usually used for long-term growth. However, the boron doping efficiency and the presence of metal impurities in BDD single crystals synthesized using these two alloy catalysts remain unclear. To reduce metal impurities in diamond and effectively dope it with boron, we investigated the influence of FeNi and FeCo alloy catalysts on boron doping of diamond. In addition, due to the crystal plane selectivity of boron entering diamond, different growth regions have different boron doping concentrations, resulting in different distributions of boron impurities in single-crystal diamond.[13,29] Therefore, we chose the (111) growth region to compare the boron doping. At the same time, (100) and (111) seed planes were used to synthesize BDD, with the (111) plane serving as the primary plane, and the boron content in its growth region was compared. Our work is of great significance for improving the performance of large, single-crystal BDD and semiconductor applications.

2. Experimental details

In this study, we synthesized single-crystal BDD using the temperature gradient method in a cubic multi-anvil press (SPD-6 × 1400) at a pressure of 5.4 GPa and a temperature of 1290–1330 °C. $Fe_{58}Ni_{42}$ and $Fe_{60}Co_{40}$ served as metal solvents. Figure 1 is a schematic diagram of the assembly of the synthetic diamond crystals. In that experiment, high-purity phosphorus flake graphite (99.99 wt%) was used as the carbon source, and high-purity TiB_2 (99.99 wt%) served as the additive. Graphite and titanium boride (TiB_2) powder were uniformly blended in various weight ratios and subsequently compacted into a carbon source. The compacted carbon source was placed into the synthetic cavity. The (111) and (100) planes of a high-quality seed crystal, approximately 1 mm in size, were chosen as the growth surfaces for the diamond. Before the synthesis experiments, the sample assembly blocks were placed in a drying oven at 120 °C for 30 min to eliminate the influence of water adsorbed on the assembly materials on the experimental results. The temperature at the center of the heater was calibrated using a double platinum–rhodium (Pt-30% Rh/Pt-6% Rh) thermocouple based on the relation between input power and temperature. The synthetic pressure was calibrated using the calibration curves of oil pressure and chamber pressure based on the high-pressure phase transition points of bismuth (Bi), barium (Ba), and thallium (Tl).

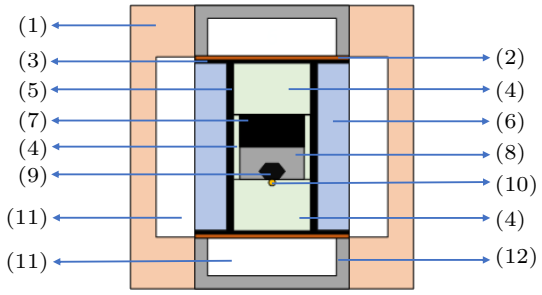


Fig. 1. Assembly for boron-doped diamond synthesis. (1) Pyrophyllite pressure medium. (2) Copper disk. (3) Graphite disk. (4) Al_2O_3 + MgO disk. (5) Graphite heater. (6) NaCl + ZrO_2 sleeve. (7) Carbon source. (8) Metal solvent. (9) Diamond sample (grown in the experiments). (10) Seed crystal. (11) Dolomite. (12) Steel cap.

The morphology of the diamond samples was examined using a Leica M205c microscope. At the same time, their infrared absorption spectra were recorded with a Bruker Vertex 70 V Fourier transform infrared (FTIR) spectrometer, covering a range of 400–4000 cm^{-1} with a resolution of 2 cm^{-1}. The test mode was set to transmission. To ensure reliable results, a potassium bromide substrate was used as the measurement background. Crystals with high boron concentration and low light transmittance were cut into 0.2 mm-thick sheets using Sanyi green laser diamond cutting equipment (model SY-CVD11E, laser wavelength 532 nm). The recrystallized graphite produced during the cutting process was then treated with a 3:1 ratio of concentrated sulfuric acid and concentrated nitric acid to obtain clean BDD sheets for FTIR testing. The distribution of elements in the diamond was analyzed using a JSM-IT200 (A) scanning electron microscope. X-ray photoelectron spectroscopy (XPS) was used to analyze

the doping and bonding of impurity elements within the crystal. That analysis was done using a Thermo Fisher Scientific ESCALAB 250Xi instrument, which operated at a pressure of 1×10^{-9} bar and a resolution of 0.1 eV.

3. Results and discussion

3.1. Effect of solvent growth surface on boron doping

3.1.1. Effect of solvent on boron doping (FeCo and FeNi)

The (111) crystal plane of the diamonds obtained from the comparison experiments of FeCo and FeNi solvent was selected for analysis. Table 1 shows the data for eight crystals measured in the experiment. Figure 2 shows optical images of diamonds grown under various solvents and various additive ratios of TiB_2. At a TiB_2 additive concentration of 2 wt%, the crystals had a yellowish color and moderate light transmittance. As the additive ratio increased to 3 wt%, the crystals darkened in color, having yellow-green hues. Some areas appeared even darker, likely due to uneven boron doping. The diamonds synthesized with the FeCo solvent at those two additive ratios were slightly darker in color compared to those produced using the FeNi solvent. When the TiB_2 additive ratio increased to 4 wt%, the crystals turned entirely black. It was evident that as the additive ratio increased, the crystal color gradually darkened and light transmittance decreased, which could be attributed to the rising boron content. Although low-doped crystals exhibited some light transmittance, diamonds grown under the FeCo solvent were darker in color. It could be initially inferred that the boron content in crystals synthesized using the FeCo solvent was higher at the same additive ratio.

Table 1. Crystals corresponding to various proportions of TiB_2 addition in FeCo–C and FeNi–C systems.

Crystal No.	Solvent	Additive ratio (wt% TiB_2)	Crystal color	Nitrogen content (ppm)	Nitrogen ion content (ppm)
A	FeCo	2	yellow	97	22
b	FeCo	3	yellow-blue	9	31
c	FeCo	4	black	–	–
d	FeCo	5	black	–	–
e	FeNi	2	yellow	124	28
f	FeNi	3	yellow-blue	75	53
g	FeNi	4	black (blue)	–	–
h	FeNi	5	black	–	–

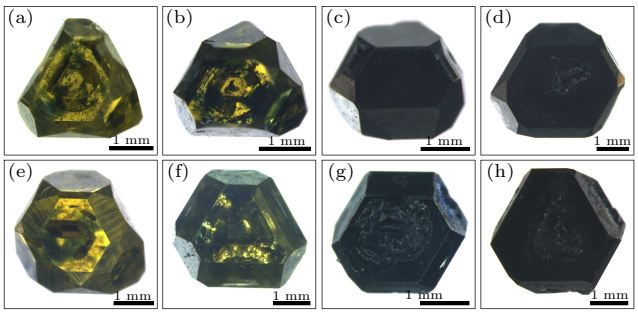


Fig. 2. Optical images of crystals synthesized by adding different concentrations of TiB_2 under FeCo–C and FeNi-C systems. (a) FeCo-2 wt% TiB_2. (b) FeCo-3 wt% TiB_2. (c) FeCo-4 wt% TiB_2. (d) FeCo-5 wt% TiB_2. (e) FeNi-2 wt% TiB_2. (f) FeNi-3 wt% TiB_2. (g) FeNi-4 wt% TiB_2. (h) FeNi-5 wt% TiB_2.

To further assess the boron content, we conducted FTIR spectrometer testing on eight diamonds. Due to the different boron concentrations in the (100) and (111) growth regions, we selected the (111) growth region of the sampled as the region for FTIR spectroscopy testing. A minimum of five measurements were taken for each diamond, from which three representative points were selected for analysis. The FTIR spectra of diamonds synthesized with TiB_2 additions of 2 wt% and 3 wt% using two solvents, along with their corresponding test points, are shown in Fig. 3. The peak at 1290 cm^{-1} (D′ center)[30] was the result of infrared absorption induced by boron-related impurities in the diamond. The peaks at 2460 cm^{-1} and 2800 cm^{-1} were attributed to the first and second excited states of electronic transitions at the acceptor energy level, respectively.

At a TiB_2 content of 2 wt%, the crystals grown under both solvents had distinct diamond characteristic peaks at 1970 cm^{-1}, 2030 cm^{-1}, and 2160 cm^{-1}. With the increase in B concentration, the characteristic peak of boron became increasingly obvious, overshadowing the characteristic peak of diamond. Therefore, when the boron concentration reached a certain height, the diamond peak was not obvious.[31] Figure 3(a) shows the FTIR absorption curve of the crystal grown using the FeCo solvent. The N^+ correlation peak at 1332 cm^{-1} is relatively weak, whereas a single-phonon absorption peak of boron is present at 1290 cm^{-1}. Also, boron-related peaks appear at 2460 cm^{-1} and 2800 cm^{-1}. That occurred due to the presence of excess boron acceptors remaining after the compensation of boron and nitrogen. The test points indicated in the optical diagram, along with their corresponding FTIR absorption curves, show that boron peaks varied at different positions within the same diamond. The boron peaks at 2460 cm^{-1} for point 3 in Fig. 3(a) are weaker than those at points 1 and 2, and the peaks at 2800 cm^{-1} are nearly absent. The optical diagram of the diamond shows that the colors at points 1 and 2 are darker than at point 3. In Fig. 3(b), the FTIR absorption curve

of the diamond synthesized using the FeNi solvent displays no neutral boron-related peaks at 2460 cm^{-1} and 2800 cm^{-1}; only the N-related peak at 1332 cm^{-1} is present. That phenomenon was attributed to the compensatory interaction between boron and nitrogen, which facilitated the formation of N^+.[32] That suggested that the diamond contained negligible electrically neutral boron impurities, because all boron acceptors were compensated by nitrogen. Adding 2 wt% TiB_2 introduced two impurities, nitrogen and boron, in the BDD grown using two solvents. Nitrogen acted as a donor impurity, supplying electrons to the acceptor impurity boron and transforming into N^+. That phenomenon is known as the compensation effect, where donor and acceptor impurities neutralize each other.

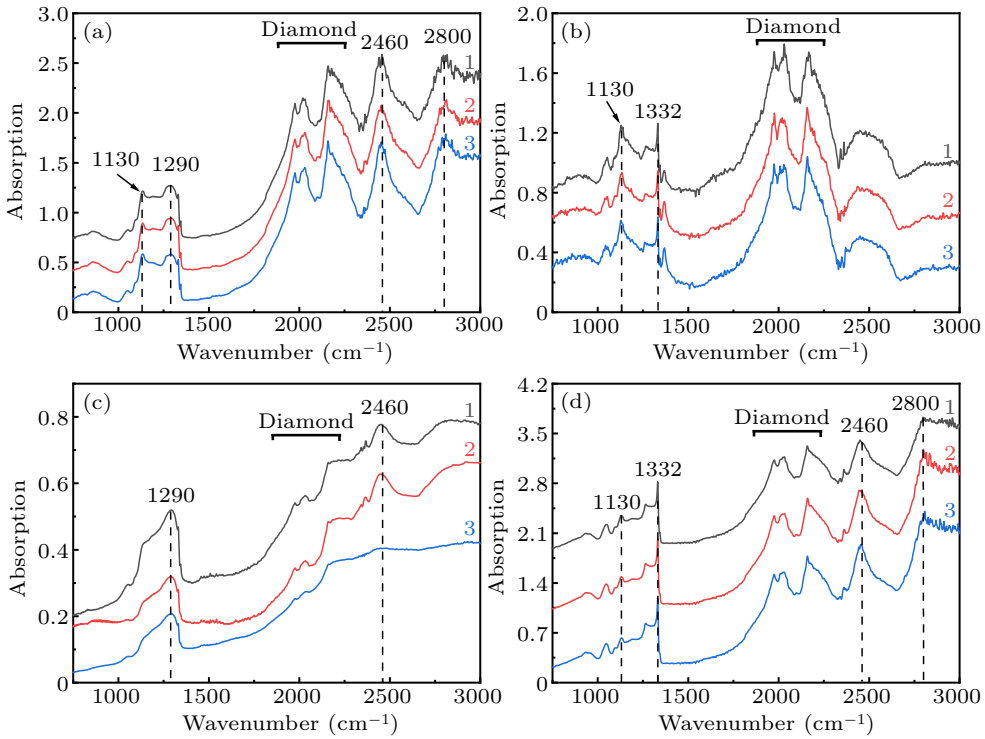


Fig. 3. FTIR spectra of corresponding points of 2 wt% and 3 wt% TiB_2 addition crystals under FeCo and FeNi solvents. (a) 2 wt% TiB_2-FeCo. (b) 2 wt% TiB_2-FeNi. (c) 3 wt% TiB_2-FeCo. (d) 3 wt% TiB_2-FeNi.

When the proportion of TiB_2 additive increased to 3 wt%, the characteristic peak of boron became more obvious, and the characteristic peak of diamond appeared less obvious. As shown in Fig. 3(c), the crystal synthesized under FeCo solvent completely lost its N^+ peak at 1332 cm^{-1}, and the diamond characteristic peak also appeared less conspicuous. In comparison to the 2 wt% addition crystal shown in Fig. 3(a), the boron peak at 1290 cm^{-1} in the crystal shown in Fig. 3(c) is significantly intensified, whereas the boron peak at 2460 cm^{-1} is less pronounced. That observation indicated that boron concentration increased with a higher additive ratio. Figure 3(d) shows that the FTIR spectra of the crystals synthesized under the FeNi solvent at the three marked positions are quite similar. In contrast, the FTIR spectra of crystals synthesized under FeNi solvent under the same conditions at three labelled positions are very similar (Fig. 3(d)), with crystals showing a weak boron peak at 1290 cm^{-1} and a strong N^+ peak at 1332 cm^{-1}. That was because there was not enough B in the crystal to form a peak at 1290 cm^{-1}, so most of the B combined with N to form a N^+ peak at 1332 cm^{-1}. That indicated that when 3 wt% TiB_2 was added, the boron content in the crystals grown with the FeNi solvent was significantly lower than that in the FeCo solvent. At a low additive concentration of 2–3 wt% TiB_2, the N^+ ions in the BDD grown using the FeNi solvent were significantly more abundant than those in diamonds produced by the FeCo solvent. That suggested that the FeCo solvent was more effective for achieving efficient boron doping.

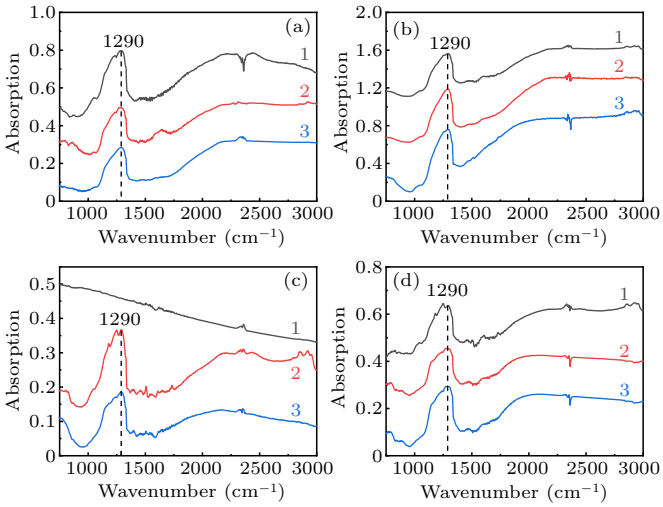


Fig. 4. FTIR spectra of corresponding points of 4 wt% and 5 wt% TiB_2 addition crystals under FeCo and FeNi solvent. (a) 4 wt% TiB_2-FeCo. (b) 4 wt% TiB_2-FeNi. (c) 5 wt% TiB_2-FeCo. (d) 5 wt% TiB_2-FeNi.

As the boron doping level increased, the light transmittance of the crystal declined. In our testing, we used diamond-cut sheets. Figure 4 shows the sheet diagram and the results of the FTIR absorption spectra. The FTIR absorption spectra obtained from diamond flakes showed that when the TiB_2 addition exceeded 4 wt%, the N-related peaks in diamonds from both the FeCo and FeNi solvents disappeared completely, leaving only the B-related peaks. That indicated that the nitrogen content in the diamonds vanished once a certain doping concentration was reached for both solvents. At a TiB_2 addition level of 4 wt%, both crystals grown in the FeCo solvent (Fig. 4(a)) and those grown in the FeNi solvent (Fig. 4(b)) had pronounced boron peaks at 1290 cm^{-1}. The crystal shown in Fig. 4(a) had a strong absorption peak at 2460 cm^{-1}, whereas the crystal in Fig. 4(b) lacked measurable peaks at both 2460 cm^{-1} and 2800 cm^{-1}. That difference further indicated that the diamond grown under the FeCo solvent contained a higher concentration of boron. At a TiB_2 additive ratio of 5 wt%, the FTIR absorption spectrum of diamond grown under the FeCo solvent (Fig. 4(c)) had strong boron peaks at 1290 cm^{-1} in addition to curves 2 and 3, particularly noted at point 1. The FTIR absorption curve has a diagonal trend, indicating an excessive concentration of boron. Unlike the BDD grown under the FeNi solvent (Fig. 4(d)), which did not have a similar diagonal trend, the absorption characteristics resemble those at points 2 and 3 of the diamond grown in the FeCo solvent (Fig. 4(c)). Notably, the boron peak in Fig. 4(c) is stronger than that in Fig. 4(d). To achieve a more accurate measurement of boron content, we calculated the boron concentration using the absorption coefficient of the single-phonon absorption peak at 1290 cm^{-1}. The equation is

$$[B] \approx 1.67 \times 10^{17} \alpha_{1290}, \tag{1}$$

where $[B]$ is the boron impurity concentration in units of cm^{-3}, and α_{1290} is the absorption coefficient of the monophonon absorption peak. The uncertainty associated with this equation is $\pm 20\%$.[33,34] To facilitate a clearer comparison of boron doping across different solvents, we uniformly selected the darker color regions to assess boron content. A histogram was then created to visually compare the boron concentration between the two solvents as the TiB_2 additive ratio increased (Fig. 5). More information on boron content is shown in Table S1 of the supplementary material. The FTIR spectrum effectively indicated changes in boron concentration within the diamond. Although the method for calculating boron concentration from the spectrum had a significant margin of error, it still enabled comparisons of boron levels or provided an estimated concentration range. The results indicated that the boron concentration in diamonds grown in the FeCo solvent was generally higher than in the FeNi solvent, showing consistent variations. According to previous reports, the different boron doping levels in diamond might be due to the interaction between metal elements (Co, Ni) and B during the synthesis process, resulting in different abilities to form boron compounds, leading to differences in boron content in the diamond.[26,27]

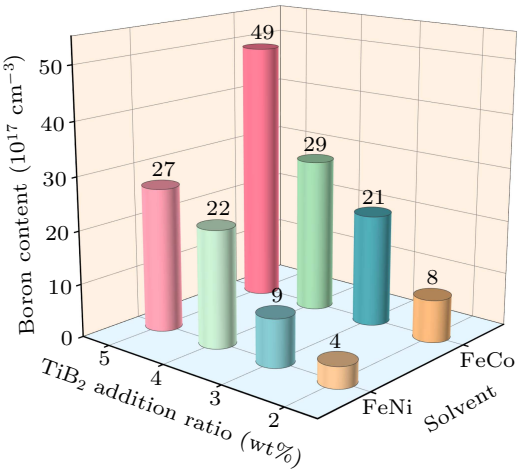


Fig. 5. Boron concentration in diamond synthesized by adding TiB_2 to FeCo and FeNi solvents.

3.1.2. Effect of growth surface on boron doping

Furthermore, in the same experiment, we synthesized crystals using the (111) and (100) seed planes as their respective growth planes. Figure 6 is a perspective view of two crystals grown under the same higher temperature and pressure conditions. It is known that with an increase in temperature, the growth rate of the diamond (100) crystal plane gradually accelerates, whereas that of the (111) crystal plane gradually slows, which is consistent with the principle of "slow surface exposure and fast surface immersion" of the Bravais law in crystal growth.[35] Because the experimental synthesis conditions were in the high-temperature region, the diamonds grown using both (100) and (111) seed planes had well-developed (111) surfaces. We conducted infrared testing on the (111) growth regions of those two crystals.

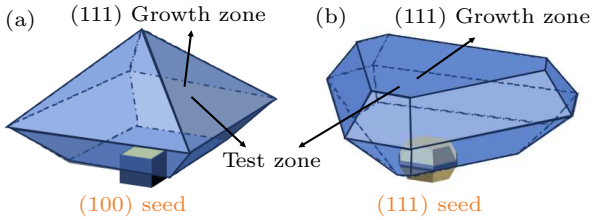


Fig. 6. (a) Three-dimensional schematic of crystals grown using the (100) seed plane at high temperature. (b) Three-dimensional schematic of crystals grown using the (111) seed plane at high temperature.

There might have been temperature differences at different positions within the same synthesis chamber.[36] We used the finite element method to simulate the temperature and convection fields of FeCo solvent under diamond synthesis pressure and temperature conditions. The simulation results are shown in Figs. 7(b) and 7(c), indicating that the solvent had completely axisymmetric temperature and convection fields. To avoid the influence of temperature on the boron content in the crystal, we arranged the two seed crystals symmetrically

along the central axis of the solvent to ensure that the temperature conditions for the growth of the two diamond crystals were the same. Figure 7(d) is a schematic diagram of the seed crystal arrangement and diamond growth. We observed that the crystals grown in the subsequent experiment, despite being subjected to the same *P*–*T* conditions, TiB_2 addition amount, and solvent, had differences. Figures 7(e) and 7(f) show optical images of crystals obtained from various seed growth surfaces in the same experiment using an FeCo solvent addition with 3 wt% TiB_2. The crystal grown from the (111) seed appears yellow, whereas the crystal grown from the (100) seed appears clearly black. The color difference was due to the varying doping levels of boron. To further investigate the incorporation of boron into diamond, we conducted FTIR tests on both crystals. As shown in (111)-1 and (111)-2 in Fig. 7(g), the FTIR absorption curves of the crystal have a prominent diamond absorption peak alongside a N^+ peak at 1332 cm^{-1}. Additionally, the boron peak at 1290 cm^{-1} is less pronounced, likely due to compensation by nitrogen. Furthermore, boron peaks are also shown at 2460 cm^{-1} and 2800 cm^{-1}. In the crystal grown from the (100) seed crystal, in contrast, the diamond characteristic peak is very weak and almost invisible relative to the boron peak. Instead, there is a distinct single-phonon absorption peak for boron impurity at 1290 cm^{-1}, along with the first excited state of the acceptor level observed at 2460 cm^{-1}. This phenomenon can be attributed to the higher boron content in the crystals shown in Fig. 7(f).

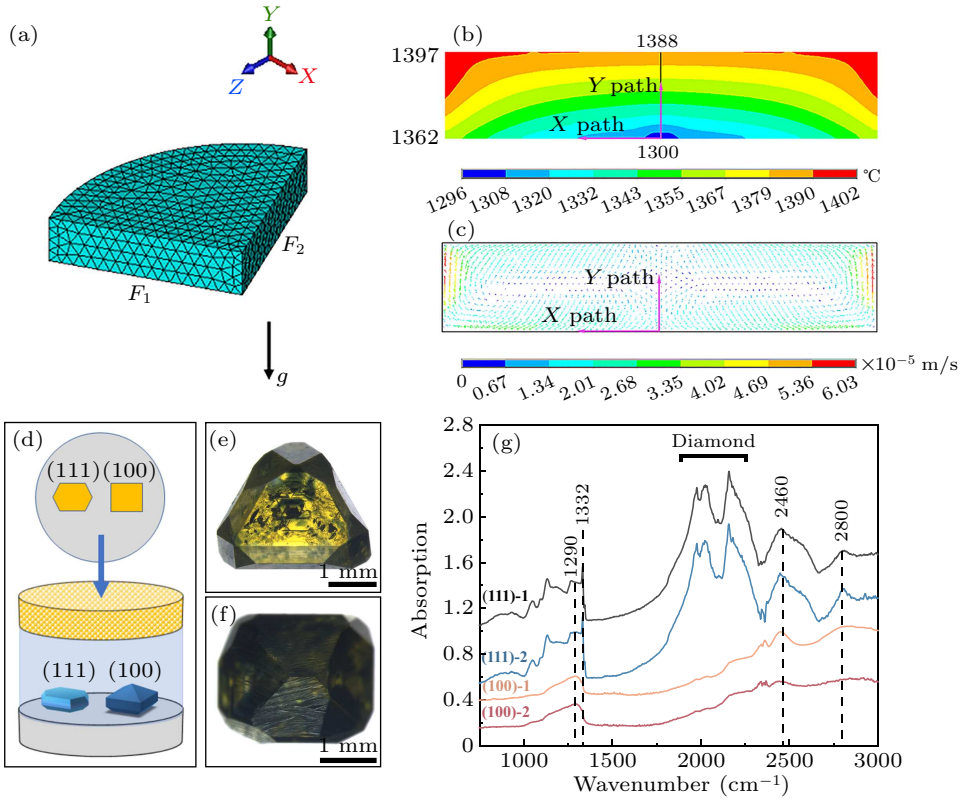


Fig. 7. (a) The 1/4 FeCo solvent geometric model. (b) Simulation result of temperature and convection fields. (c) Simulation result of the FeCo solvent. (d) Schematic diagram of seed crystal and crystal growth. (e) (111) crystal optical diagram. (f) (100) crystal optical pattern. (g) Infrared absorption spectra of (111) and (100) crystals.

Table 1. Experimental conditions and results of FeCo-3 wt% TiB_2 addition (111) and (100) crystals.

Crystal No.	Seed plane	Color	Morphology	(111) growth zone		
				Nitrogen content (ppm)	Nitrogen ion content (ppm)	Boron content (10^{17} cm^{-3})
D-1	(111)	yellow	plate crystal	91	30	7
D-2	(100)	yellow-blue	tower crystal	–	–	30

Similar to our earlier comparison of the FeCo and FeNi solvents, we estimated the boron concentration in this group of diamond crystals. Results are shown in Table 2. The calculation shows that the boron content of the (111) crystals grown using the (100) seed plane was higher. The calculation results of boron content with 2 wt%, 4 wt%, and 5 wt% TiB_2 addition ratios also obtained consistent conclusions. See the supplementary material for more details (Fig. S1, Table S2). That finding did not contradict previous studies, which indicated that the boron content in the (111) crystal plane is higher than in the (100) plane at the same additive ratio. In this experiment, the crystal grown from the (100) seed consisted primar-

ily of the (111) plane and was classified as a high-temperature crystal. It might be inferred that the boron content in diamonds grown from different seed crystals in the same experiment might vary.

3.2. Effect of solvent on incorporation of metal impurities

3.2.1. Metal impurity speciation (XPS)

Additionally, to analyze the types of impurity elements and their bonding modes in BDD grown with two metals, we conducted high-resolution XPS spectral tests on C, Fe, Ni, and Co in the diamonds. To ensure the accuracy of our experimental data and minimize the effect of surface impurities, we laser-cut the sample into a single wafer and selected an area free from inclusions for testing. Figure 8 shows a high-resolution XPS scan of (111) and (100) crystal additions with 4 wt% TiB_2 under two solvents. The C 1s energy levels for all four crystals had three secondary peaks at 284.5 eV, 285.8 eV, and 288.2 eV, corresponding to sp^2 C–C, sp^3 C–C, and C–O bonds, respectively.[37–39] The secondary peaks associated with the sp^3 C–C bonds progressively increased from crystal 8-(a) to crystal 8-(d). Among the four crystals, crystal 8-(a) had the strongest Fe 2p energy level, whereas the Fe 2p energy levels for crystals 8-(b) and 8-(c) were weaker, each containing six secondary peaks. In addition to the satellite peaks, the secondary peaks at 707.3 eV and 720.6 eV were

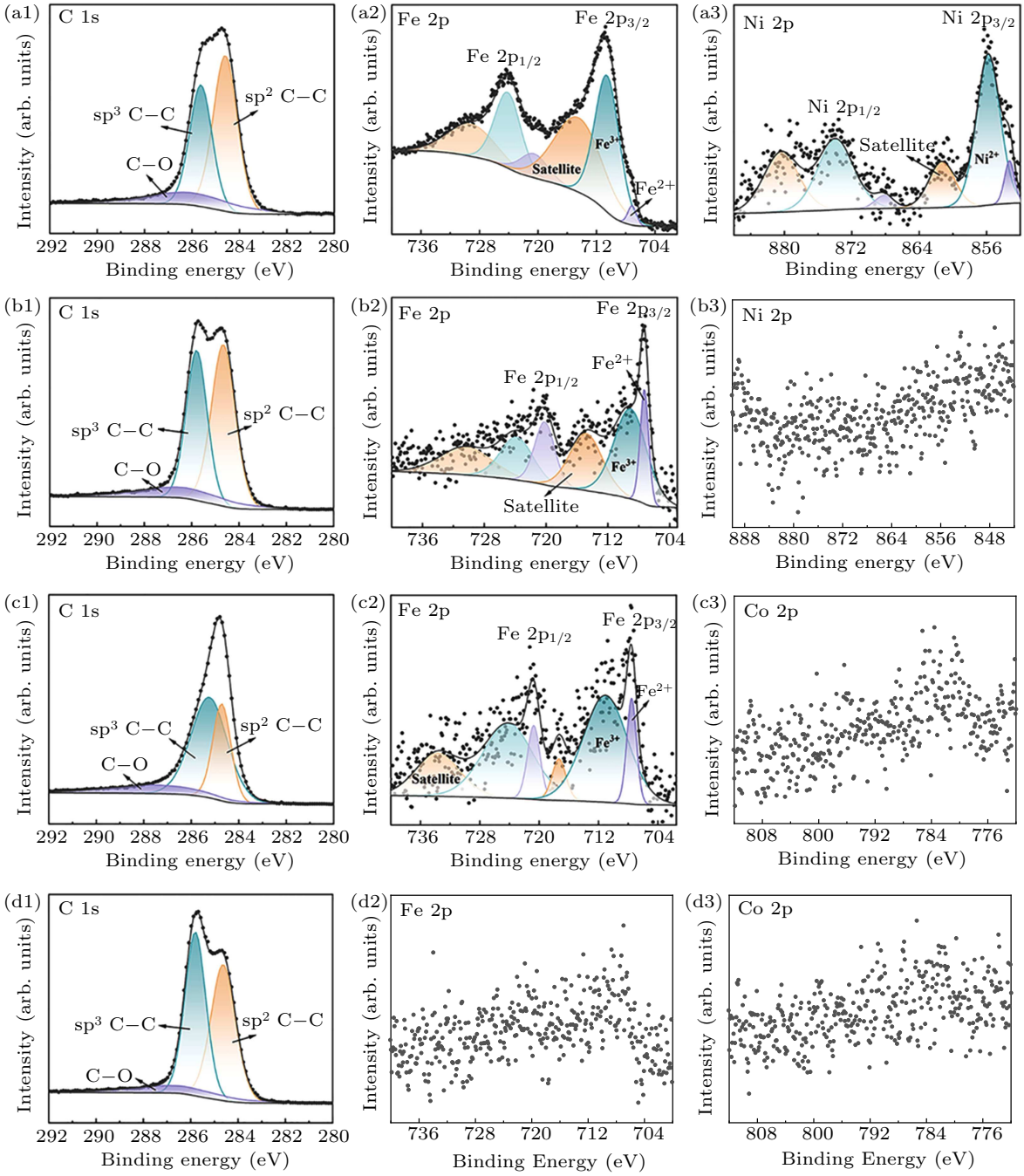


Fig. 8. XPS spectra of BDD grown with two different solvents with 4 wt% TiB_2. (a) FeNi-(100). (b) FeNi-(111). (c) FeCo-(100). (d) FeCo-(111).

associated with Fe^{2+} ions. The Fe 2p secondary peaks appeared primarily at 710.6 eV and 724.1 eV, corresponding to Fe $2p_{3/2}$ and Fe $2p_{1/2}$ respectively, which were related to Fe^{3+} ions.[40–43] The high-resolution Fe 2p energy level of crystal 8-(d) showed no distinct bonding modes. Additionally, the Fe 2p energy level in the FeCo solvent was lower than that in the FeNi solvent. Among the crystals grown using the FeNi solvent, the Ni 2p secondary peaks in crystal 8-(a) appeared primarily at 873 eV and 856 eV, corresponding to Ni $2p_{1/2}$ and Ni $2p_{3/2}$, respectively.[41,44–46] Fitting analysis showed a total of six secondary peaks. In addition to the satellite peaks, the secondary peaks at 853.4 eV and 868.2 eV were linked to NiO, whereas the peaks at 855.8 eV and 874 eV corresponded to $Ni(OH)_2$. Notably, no Ni 2p levels were detected in crystal 8-(b). Similarly, in the FeCo solvent, no Co 2p energy levels were observed in either crystal 8-(c) or crystal 8-(d). The XPS data indicated that Fe and Ni impurity atoms in BDD synthesized with the FeNi solvent were incorporated into the crystal more readily. In contrast, BDD synthesized using the FeCo solvent contained lower levels of Fe impurities, and no Co impurities were detected. Based on the energy dispersive x-ray spectroscopy (EDS) spectrum, we concluded that the FeCo solvent was more suitable for growing BDD single crystals.

3.2.2. Metal impurity concentration (energy dispersive x-ray spectroscopy)

To investigate the entry and distribution of metal impurities in the diamonds, we selected areas free from metal inclusions for EDS scans on 4 wt% TiB_2-addition (100) and (111) crystals across two solvents. We then analyzed the elemental distribution within the diamond flakes (Fig. 9). After scanning the (100) crystal (a) and (111) crystal (b) of the FeNi solvent, we observed that, in addition to the predominant distribution of C, small amounts of Fe and Ni were also present. In comparison to Fe, Ni is incorporated more readily into BDD. However, neither Fe nor Co was detected in the FeCo solvent, regardless of whether the (100) or (111) seed crystal was used. That indicated that crystals in the FeNi solvent were more susceptible to metal impurities. In contrast, those in the FeCo solvent tended to be purer, facilitating the growth of high-quality BDD single crystals.

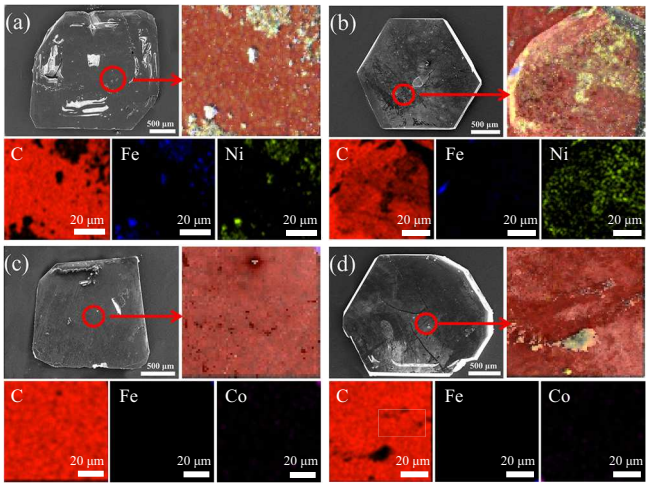


Fig. 9. SEM image and energy dispersive x-ray spectroscopy elemental mappings of 4 wt% TiB_2 addition crystals under FeCo and FeNi solvents. (a) FeNi-(100). (b) FeNi-(111). (c) FeCo-(100). (d) FeCo-(111).

4. Conclusion

In summary, our results indicated that at the same TiB_2 additive ratio, boron-doped diamonds grown on (100) and (111) diamond seeds using the FeCo solvent system had consistently higher boron doping concentrations than those using the FeNi solvent system. That difference might have been related to factors such as the solubility and activity of boron in FeCo alloys, interfacial properties, or solvent stability. Systematic investigation of the effects of solvent composition gradients will be the focus of future work.

Additionally, our findings showed that the boron content in the (111) growth zone in diamonds varied when synthesized using different seed growth planes, even under the same growth pressure, temperature, and time. Additionally, the crystals grown with FeCo solvent had fewer metal impurities, demonstrating superior effectiveness in impurity removal. The FeCo solvent effectively doped boron, establishing a strong foundation for the subsequent production of high-quality BDD single-crystal semiconductors. Our research findings are significant for selecting solvents and seed growth planes in the preparation of p-type diamond semiconductors using the HPHT method.

Acknowledgements

The project was supported by the National Natural Science Foundation of China (Grant Nos. 12274373 and 12274372), the Natural Science Foundation of Henan Province (Grant Nos. 242300421155 and 252300421475), the Key Research Projects of Higher Education Institutions in Henan Province (Grant No. 25A140008), the Natural Science Foundation of Chongqing, China (Grant Nos. CSTB2023NSCQ-LZX0100 and CSTB2023NSCQ-MSX0362), Central Plains Science and Technology Innovation Youth Top Notch Talents, and Independent Innovation Project for Graduate Students of Zhengzhou University (Grant No. 20250450).

References

[1] Zhang J G, Wang X C, Shen B and Sun F H 2013 *Int. J. Refract. Met. Hard Mat.* **41** 285
[2] Zhao Y S, Yan F Y and Liu X 2023 *Diam. Relat. Mat.* **136** 110016
[3] Calzaferri G and Rytz R 1996 *J. Phys. Chem.* **100** 11122
[4] Grot S A, Hatfield C W, Gildenblat G S, Badzian A R and Badzian T 1991 *Appl. Phys. Lett.* **58** 1542
[5] Verhoeven H, Boettger E, Flöter A, Reiss H and Zachai R 1997 *Diam. Relat. Mat.* **6** 298
[6] Mudryi A V, Larionova T P, Shakin I A, Gusakov G A, Dubrov G A and Tikhonov V V 2004 *Semiconductors* **38** 520

[7] Fedoseev D V, Vnukov S P, Bukhovets V L and Anikin B A 1986 *Surf. Coat. Technol.* **28** 207

[8] Perez G, Marechal A, Chicot G, Lefranc P, Jeannin P O, Eon D and Rouger N 2020 *Diam. Relat. Mat.* **110** 108154

[9] Raynaud C, Tournier D, Morel H and Planson D 2010 *Diam. Relat. Mat.* **19** 1

[10] Li S S, Ma H A, Li X L, Su T C, Huang G F, Li Y and Jia X P 2011 *Chin. Phys. B* **20** 028103

[11] Zhao X, Liu Y M, Liu L S, Song H Z, Hu T W, Lan J Y, Zhai Z F, Li D K, Wang C, Chen B, Jiang X and Huang N 2024 *Ceram. Int.* **50** 33868

[12] Naoi S, Natsui K and Einaga Y 2016 *Meet. Abstr.* **MA2016-02** 3585

[13] Wang Z W, Wang Z Q, Liu Y, Zhao H, Li B W, Guo Q Y, Xu A K, Ma H A, Chen L C and Jia X P 2024 *Int. J. Refract. Met. Hard Mat.* **120** 106608

[14] Lei Q S, Wu Z M, Geng X H, Zhao Y, Sun J and Xi J P 2006 *Chin. Phys. B* **15** 213

[15] Hao L C, Chen Z A, Liu D Y, Zhao W K, Zhang M, Tang K, Zhu S M, Ye J D, Zhang R and Zheng Y D 2023 *Chin. Phys. B* **32** 038101

[16] Ren Y, Li X G, Lv W, Dong H Y, Cheng Q H, Yue F, Wöhrl N, Mendes J C, Yang X and Li Z X 2024 *J. Mater. Sci. Mater. Electron.* **35** 525

[17] Teng Y, Liu D Y, Tang K, Zhao W K, Chen Z A, Huang Y M, Duan J J, Bian Y, Ye J D and Zhu S M 2022 *Chin. Phys. B* **31** 128106

[18] Shang H and Jiang Y F 2024 *Semicond. Sci. Technol.* **39** 115013

[19] Fujita N, Blumenau A T, Jones R, Öberg S and Briddon P R 2006 *Phys. Status Solidi A* **203** 3070

[20] Ichikawa K, Shimaoka T, Kato Y, Koizumi S and Teraji T 2020 *J. Appl. Phys.* **128** 155302

[21] Yin L W, Li M S, Sun D S, Gong Z G, Yao Z Y, Cui J J and Hao Z Y 2001 *J. Mater. Sci.* **36** 5585

[22] Srimongkon K, Ohmagari S, Kato Y, Amomkitbamrung V and Shikata S ichi 2016 *Diam. Relat. Mat.* **63** 21

[23] Xie L, Yoneda A, Yoshino T, Yamazaki D, Tsujino N, Higo Y, Tange Y, Irifune T, Shimei T and Ito E 2017 *Rev. Sci. Instrum.* **88** 093904

[24] Ekimov E A, Sidorov V A, Bauer E D, Mel'nik N N, Curro N J, Thompson J D and Stishov S M 2004 *Nature* **428** 542

[25] Xie L, Yoneda A, Yoshino T, Fei H and Ito E 2016 *High Press. Res.* **36** 105

[26] Chen L C, Miao X Y, He X M, Guo L S, Fang S, Wang Y, Wang Z K, Fang C, Ma H A and Jia X P 2018 *J. Cryst. Growth* **498** 67

[27] Ekimov E A, Sidorov V A, Maslakov K, Sirotinkin B P, Krotova M D and Pleskov Y 2018 *Diam. Relat. Mat.* **89** 101

[28] Ekimov E A, Sidorov V A, Chtchelkatchev N M, Lyapin S G and Khmelnitsky R A 2024 *Diam. Relat. Mat.* **142** 110784

[29] Mortet V, Taylor A, Lambert N, Gedeonova Z, Fekete L, Lorincik J, Klimsa L, Kopecek J, Hubik P, Soban Z, Laposa A, Davydova M, Voves J, Posta A, Povolny V and Hazdra P 2021 *Diam. Relat. Mat.* **111** 108223

[30] Chepurov A I, Yelisseyev A P, Zhimulev E I, Sonin V M, Fedorov I I and Chepurov A A 2008 *Inorg. Mater.* **44** 377

[31] Panov M, Zubkov V, Solomnikova A and Klepikov I 2024 *Mater. Sci. Eng: B* **303** 117334

[32] Lawson S C, Fisher D, Hunt D C and Newton M E 1998 *J. Phys.: Condens. Matter* **10** 6171

[33] Miao X Y, Chen L C, Ma H A, Fang C, Guo L S, Fang S, Wang Y and Jia X P 2018 *Cryst. Eng. Comm* **20** 7109

[34] Blank V D, Kuznetsov M S, Nosukhin S A, Terentiev S A and Denisov V N 2007 *Diam. Relat. Mat.* **16** 800

[35] Strong H M and Chrenko R M 1971 *J. Phys. Chem.* **75** 1838

[36] Li Y D, Cheng Y S, Su M J, Ran Q F, Wang C X, Ma H A, Fang C and Chen L C 2020 *Chin. Phys. B* **29** 078101

[37] Veyan J F, De Obaldia E, Alcantar-Peña J J, Montes-Gutierrez J, Arellano-Jimenez M J, José Yacaman M and Auciello O 2018 *Carbon* **134** 29

[38] Rani R, Panda K, Kumar N, Sankaran K J, Ganesan K and Lin I N 2018 *J. Phys. Chem. C* **122** 8602

[39] Liu X B, Chen X, Ma H A, Jia X P, Wu J S, Yu T, Wang Y B, Guo J G, Petitgirard S, Bina C R and Jacobsen S D 2016 *Sci. Rep.* **6** 30518

[40] Lei D Y, Liu C K, Dong C L, Wang S J, Zhang P, Li Y, Liu J X, Dong Y L and Zhou C X 2024 *ACS Appl. Nano Mater.* **7** 25259

[41] Li G, Wang B D, Sun Q, Xu W Q and Han Y F 2019 *J. Nanosci. Nanotechnol.* **19** 3343

[42] Conradie J and Erasmus E 2016 *Polyhedron* **119** 142

[43] Wang Y H, Wu L M, Qu K G and Li B T 2025 *Fuel* **380** 133072

[44] Ma C Y, He H X, Zhang H B, Xia F F and Li H X 2025 *Surf. Coat. Technol.* **496** 131641

[45] Wang X Y, Jiang Y, Wang S S, Zhang L Y, Zhang T H and He P 2024 *Microchem J.* **201** 110692

[46] Bagus P S, Nelin C J, Mergelsberg S T, Lahiri N and Ilton E S 2024 *J. Chem. Phys.* **161** 164701